

# Supersymmetry Searches in GUT Models with Non-Universal Scalar Masses

M. Cannoni<sup>\*1</sup>, J. Ellis<sup>†2,3</sup>, M. E. Gómez<sup>‡1</sup>, S. Lola<sup>§4</sup>, and R. Ruiz de Austri<sup>¶5</sup>

<sup>1</sup>Departamento de Física Aplicada, Facultad de Ciencias Experimentales,  
Universidad de Huelva, 21071 Huelva, Spain

<sup>2</sup>Theoretical Particle Physics and Cosmology Group, Physics Department, King's College London,  
London WC2R 2LS, UK

<sup>3</sup>TH Division, Physics Department, CERN CH-1211 Geneva 23, Switzerland

<sup>4</sup>Department of Physics, University of Patras, 26500 Patras, Greece

<sup>5</sup>Instituto de Física Corpuscular, IFIC-UV/CSIC, Valencia, Spain

KCL-PH-TH/2015-52, LCTS/2015-39, CERN-PH-TH/2015-271,  
UHU-FISUM/2015-17, IFIC/15-89

## Abstract

We study SO(10), SU(5) and flipped SU(5) GUT models with non-universal soft supersymmetry-breaking scalar masses, exploring how they are constrained by LHC supersymmetry searches and cold dark matter experiments, and how they can be probed and distinguished in future experiments. We find characteristic differences between the various GUT scenarios, particularly in the coannihilation region, which is very sensitive to changes of parameters. For example, the flipped SU(5) GUT predicts the possibility of  $\tilde{t}_1 - \chi$  coannihilation, which is absent in the regions of the SO(10) and SU(5) GUT parameter spaces that we study. We use the relic density predictions in different models to determine upper bounds for the neutralino masses, and we find large differences between different GUT models in the sparticle spectra for the same LSP mass, leading to direct connections of distinctive possible experimental measurements with the structure of the GUT group. We find that future LHC searches for generic missing  $E_T$ , charginos and stops will be able to constrain the different GUT models in complementary ways, as will the Xenon 1 ton and Darwin dark matter scattering experiments and future FERMI or CTA  $\gamma$ -ray searches.

---

\*email: mirco.cannoni@dfa.uhu.es

†email: John.Ellis@cern.ch

‡email: mario.gomez@dfa.uhu.es

§email: magda@physics.upatras.gr

¶email: rruiz@ific.uv.es

# Contents

<b>1</b>	<b>Introduction</b>	<b>2</b>
<b>2</b>	<b>Relevant Features of Supersymmetric GUT Models</b>	<b>3</b>
<b>3</b>	<b>Sampling Methodology and Constraints</b>	<b>4</b>
<b>4</b>	<b>Non-Universality Parameters and Relic Density Mechanisms</b>	<b>6</b>
<b>5</b>	<b>Relic Density, Higgs Mass and <math>\delta a_\mu^{SUSY}</math></b>	<b>9</b>
<b>6</b>	<b>Direct and Indirect Dark Matter Searches</b>	<b>11</b>
<b>7</b>	<b>LHC Searches</b>	<b>12</b>
<b>8</b>	<b>Summary and Conclusions</b>	<b>16</b>

## 1 Introduction

The recent years have provided a plethora of new experimental and cosmological information that provides important constraints on possible extensions of the Standard Model (SM). Recent LHC results, including the Higgs measurements [1, 2, 3, 4], severely constrain some of the simplest scenarios. We know, however, that there must be some physics beyond the SM. For example, massive neutrinos cannot be accommodated within the SM, nor can the observed baryon asymmetry of the universe or the origin of Cold Dark Matter (CDM) be explained. In looking for possible extensions of the SM that address these issues, supersymmetry (SUSY) continues to provide significant theoretical advantages, especially if we believe in unification beyond the SM. Most notably for the purposes of this paper, the lightest supersymmetric particle (LSP) can explain the origin of CDM [5, 6].

Reconciling the amount of CDM deduced from the data of the Wilkinson Microwave Anisotropy Probe (WMAP) [7, 8] and the Planck satellite [9, 10] with the predictions of supersymmetric models, has been a major challenge in recent years. Although the minimal constrained supersymmetric extension of the SM (CMSSM) is still compatible with the LHC and WMAP predictions [11], the allowed parameter space is severely constrained, since a Higgs mass  $m_h \sim 125$  GeV implies a relatively heavy sparticle spectrum. However, the allowed regions may change significantly in different versions of the MSSM, especially in the coannihilation strips where, e.g.,  $m_\chi \sim m_{\tilde{\tau}_1}$  or  $\sim m_{\tilde{t}_1}$ . Because of their narrow widths, these coannihilation strips are particularly sensitive to changes in the input model parameters.

In this work, we study these changes in various scenarios that go beyond the constrained minimal supersymmetric extension of the SM (CMSSM), in which soft SUSY-breaking terms are assumed to be universal at the GUT scale, using dark matter considerations as a probe of different theoretical constructions. In general, GUT scenarios that favour particular degeneracies in the sparticle spectrum will lead to additional contributions to coannihilations, thus enhancing their efficiency. Conversely, experimental signals sensitive to these degeneracies can provide information about the gauge unification group. Following previous studies of models with non-universal soft SUSY-breaking Higgs mass parameters (NUHM1,2) [12, 13, 14, 15, 16], we analyse the predictions of various SUSY GUT models, including SO(10) [17, 18, 19, 20, 21], minimal SU(5) [22, 23] and flipped SU(5) [24, 25, 26, 27].

Our paper is structured as follows: In Section 2 we review the features of GUT models that are relevant for our studies. In Section 3 we discuss our sampling methodology for searching for regions of the parameter space compatible with the data. In Section 4 we discuss the implications of non-universalities for the different mechanisms that reproduce the correct relic CDM density. In Section 5 we discuss in more detail how the results of our scans depend on the relation between the relic abundance mechanisms, the value of the Higgs boson mass and the supersymmetric contribution to  $\delta a_\mu = [(g_\mu - 2)/2]_{\text{exp}} - [(g_\mu - 2)/2]_{\text{SM}}$ . In Section 6, we present the cross sections for direct and indirect CDM detection. In Section 7, we study how sparticle searches at the LHC impose further constraints on our models. Finally, in Section 8 we summarise our results and discuss future prospects.

## 2 Relevant Features of Supersymmetric GUT Models

We assume that SUSY breaking occurs at some scale  $M_X$  above  $M_{GUT}$ , and is induced by a mechanism that generates generation-blind soft terms. Between the scales  $M_X$  and  $M_{GUT}$ , the renormalization group equations (RGE) and additional interactions associated with flavour, e.g., Yukawa interactions, might induce non-universalities in the soft terms, which we do not consider here, while the theory still preserves the GUT symmetry. Below  $M_{GUT}$ , the effective theory is the MSSM with SUSY masses that are common for fields in the same representation of the GUT group. Our approach is therefore to assume a pattern of soft terms with common soft masses for all the particles that belong to the same representations of the GUT group under consideration, while allowing different common masses for inequivalent representations.

The simplest possibility arises within an SO(10) GUT [17, 18, 19, 20, 21]. In this case, all quarks and leptons are accommodated in the same  $\mathbf{16}$  representation, while we assume that the up and down Higgs multiplets are in a pair of  $\mathbf{10}$  representations. Since this assignment also determines common sfermion mass matrices and beta functions, similar behaviour under RGE runs is to be expected. Consequently, in this GUT model there is a common soft SUSY-breaking mass for all sfermions (squarks and sleptons) and two different masses for  $m_{h_u}$  and  $m_{h_d}$ . From this point of view, the SO(10) scenario can be identified with the NUHM2 studied previously [13], and we include it as a reference for comparison with other GUT groups.

The situation changes significantly in the case of the SU(5) group [22, 23]. In this case, the multiplet assignments are as follows:

$$(Q, u^c, e^c)_i \in \mathbf{10}_i, (L, d^c)_i \in \bar{\mathbf{5}}_i, \nu_i^c \in \mathbf{1}_i. \quad (1)$$

The soft terms that we assume are the same for all the members of the same representation at the GUT scale, but are different for the  $\mathbf{10}$  and  $\bar{\mathbf{5}}$  in general, and we assume that the singlet neutrinos decouple at the GUT scale, and therefore do not affect our analysis. A similar approach was followed in [28], but the main aim of that work was to reconcile the correct prediction of  $m_h$  (requiring a heavy SUSY spectrum) with a supersymmetric contribution that could explain the discrepancy of the SM prediction for  $(g_\mu - 2)$  with its experimental value. However, the main aim of this work is to analyse the relic density predictions and to extend the full analysis also to the case of the flipped SU(5) [24, 25, 26, 27], which leads to predictions that differ significantly, and has some distinctive features. The particle assignments are different in flipped SU(5) [24, 25, 26, 27]:

$$(Q, d^c, \nu^c)_i \in \mathbf{10}_i, (L, u^c)_i \in \bar{\mathbf{5}}_i, e_i^c \in \mathbf{1}_i. \quad (2)$$

The impacts of these assignments on the evolution of sparticle masses, and hence on the coannihilation strips are discussed in detail below. As before, we assume that the singlet neutrinos have already decoupled at the GUT scale. In both SU(5) models we assume that the Higgs doublets  $H_u$  and  $H_d$  of the MSSM arise from  $\mathbf{5}$  and  $\bar{\mathbf{5}}$  SU(5) representations, respectively.

The soft SUSY-breaking scalar terms for the fields in an irreducible representation  $r$  of the unification group are parametrised as multiples of a common scale  $m_0$ :

$$m_r = x_r m_0, \quad (3)$$

while the trilinear terms are defined as:

$$A_r = Y_r A_0, \quad A_0 = a_0 m_0, \quad (4)$$

where  $Y_r$  is the Yukawa coupling associated with the representation  $r$ , and we use the standard parametrization with  $a_0$  a dimensionless factor, which we assume to be representation-independent. Since the two Higgs fields of the MSSM arise from different SU(5) representations, they have different soft masses, in general. The situation in the different GUT groups is then as follows:

- SO(10): In addition to the CMSSM parameters, we introduce two new parameters  $x_u$  and  $x_d$  defined as follows:

$$m_{16} = m_0, \quad m_{H_u} = x_u m_{16}, \quad m_{H_d} = x_d m_{16}. \quad (5)$$

Similarly, the  $A$ -terms are parametrised by:

$$A_{16} = a_0 \cdot m_0, \quad (6)$$

as in minimal SO(10) with fermion fields in a common **16** representation and two Higgs fields in different **10** representations.

- SU(5): Here we use as reference the common soft SUSY-breaking masses for the fields of the **10**,  $m_{10}$ . The masses for the other representations are then defined as:

$$m_{10} = m_0, \quad m_5 = x_5 \cdot m_{10}, \quad m_{H_u} = x_u \cdot m_{10} \quad m_{H_d} = x_d \cdot m_{10}, \quad (7)$$

and the  $A$ -terms are specified via a common mass scale:

$$A_{10,5} = a_0 m_0. \quad (8)$$

- Flipped SU(5): Here we have

$$m_{10} = m_0, \quad m_5 = x_5 \cdot m_{10} \quad m_R = x_R \cdot m_{10} \quad m_{H_u} = x_u \cdot m_{10} \quad m_{H_d} = x_d \cdot m_{10}, \quad (9)$$

where  $x_R$  refers to the SU(2)-singlet fields. Similarly, the  $A$ -terms are specified as universal:  $A_0 = a_0 \cdot m_0$ .

A similar parametrization of GUT scalar non-universality in SO(10) and SU(5) was used also in Ref. [29]. For our analysis in the following Sections we assume a common unification scale  $M_{GUT}$  defined as the meeting point of the  $g_1$  and  $g_2$  gauge couplings. The GUT value for  $g_3$  is obtained by requiring  $\alpha_s(M_Z) = 0.1187$ . Above  $M_{GUT}$  we assume a unification group that breaks at this scale. We also assume that SUSY is broken above  $M_{GUT}$  by soft terms that are representation-dependent but generation-blind.

### 3 Sampling Methodology and Constraints

We work within the three different GUT scenarios SO(10), SU(5) and flipped SU(5) described above, mapping the areas of the parameter space allowed by WMAP, Planck and other constraints onto the ratios of GUT values of the soft terms for each representation. We perform scans of the model parameter spaces using their matter representation patterns as guides for the soft scalar

terms at the GUT scale, assuming common gaugino masses. For our searches for regions of the parameter spaces compatible with the data, we use a Bayesian approach based on the `MultiNest` algorithm [30] as implemented in `SuperBayeS-v2.0` [31]. `SuperBayeS` is interfaced with `SoftSUSY 3.3.10` [32, 33] as SUSY spectrum calculator, `MicrOMEGAs 2.4` [34, 35] to compute the abundance of dark matter, `DarkSUSY 5.0.5` [36, 37] for the computation of  $\sigma_{SI}$ , `SuperIso 3.0` [38, 39] to compute  $\delta a_\mu^{\text{SUSY}}$  and  $B(D)$  physics observables, `SusyBSG 1.5` for the determination of  $BR(\bar{B} \rightarrow X_s \gamma)$  [40, 41].

The likelihood function that drives our exploration to regions of the parameter space where the model predictions fit the data well is built from the following components:

$$\begin{aligned} \ln \mathcal{L}_{\text{Joint}} = & \ln \mathcal{L}_{\text{EW}} + \ln \mathcal{L}_{\text{B}} + \ln \mathcal{L}_{\Omega_\chi h^2} \\ & + \ln \mathcal{L}_{\text{LUX}} + \ln \mathcal{L}_{\text{Higgs}} + \ln \mathcal{L}_{\text{SUSY}} + \ln \mathcal{L}_{g-2}, \end{aligned} \quad (10)$$

where  $\mathcal{L}_{\text{EW}}$  is the part corresponding to electroweak precision observables,  $\mathcal{L}_{\text{B}}$  to B-physics constraints,  $\mathcal{L}_{\Omega_\chi h^2}$  to measurements of the cosmological DM relic density,  $\mathcal{L}_{\text{LUX}}$  to the constraints from direct DM detection searches (dominated by the LUX experiment) and  $\mathcal{L}_{\text{Higgs}}$  ( $\mathcal{L}_{\text{SUSY}}$ ) to Higgs (sparticle) searches at colliders. We now discuss each component in turn:

**$\mathcal{L}_{\text{EW}}$ :** We implement the constraints on the effective electroweak mixing angle  $\sin^2 \theta_{\text{eff}}$  and the total width of the Z-boson,  $\Gamma_Z$ , from the LEP experiments [42]. For the mass of the W boson,  $m_W$ , we use the Particle Data Group value [43], which combines the LEP2 and Tevatron measurements. We assume Gaussian likelihoods for all these quantities, with means and standard deviations as given in Table II of [44].

**$\mathcal{L}_{\text{B}}$ :** We consider the following flavor observables related to B physics:  $BR(\bar{B} \rightarrow X_s \gamma)$ ,  $R_{\Delta M_{B_s}}$ ,  $\frac{BR(B_u \rightarrow \tau \nu)}{BR(\bar{B}_u \rightarrow \tau \nu)_{SM}}$ ,  $BR(\bar{B}_s \rightarrow \mu^+ \mu^-)$  and  $BR(\bar{B}_d \rightarrow \mu^+ \mu^-)$ . We assume Gaussian likelihoods for all of them, and for most of them we use the measurements shown in Table II of [44]. However, the experimental values assumed for  $BR(\bar{B}_s \rightarrow \mu^+ \mu^-)$  and  $BR(\bar{B}_d \rightarrow \mu^+ \mu^-)$  are  $(2.9 \pm 0.8) \times 10^{-9}$  and  $(3.6 \pm 1.55) \times 10^{-10}$ , respectively, where we quote the total uncertainties found by adding in quadrature the theoretical [45] and experimental [46, 47] uncertainties.

**$\mathcal{L}_{\Omega_\chi h^2}$ :** We include the constraint on the DM relic abundance from the Planck satellite, assuming that the lightest neutralino is the dominant DM component. We use as central value the result from Planck temperature and lensing data  $\Omega_\chi h^2 = 0.1186 \pm 0.0031$  [48], with a (fixed) theoretical uncertainty  $\tau = 0.012$ , following Refs. [14, 16, 61], to account for the numerical uncertainties entering in the calculation of the relic density.

**$\mathcal{L}_{\text{LUX}}$ :** For direct DM detection, we include the upper limit from the LUX experiment [49], as implemented in the `LUXCalc` code [50], including both the spin-independent and spin-dependent cross-sections in the event rate calculation. We adopt hadronic matrix elements determined by lattice QCD [51, 52].

**$\mathcal{L}_{\text{Higgs}}$ :** The likelihood for the Higgs searches has two components. The first implements bounds obtained from Higgs searches at LEP, Tevatron and LHC via `HiggsBounds` [53], which returns whether a model is excluded or not at the 95% CL. The second component constrains the mass and the production times decay rates of the Higgs-like boson discovered by the LHC experiments ATLAS [1] and CMS [2]. For this we use `HiggsSignals` [54], assuming a theoretical uncertainty in the calculation of the lightest Higgs mass of 2 GeV.

$\mathcal{L}_{\text{SUSY}}$ : The constraints from SUSY searches at LEP and Tevatron are evaluated following the prescription proposed in [55]. The present limits from the Run 1 of LHC are displayed in the corresponding Figures in Section 4.

$\mathcal{L}_{g-2}$ : We adopt for the discrepancy between the experimental value of the anomalous magnetic moment of the muon and the value calculated in the Standard Model  $\delta a_\mu^{\text{SUSY}} = (28.7 \pm 8.2) \times 10^{-9}$  [56], where experimental and theoretical errors have been added in quadrature. This corresponds to a  $3.6\sigma$  discrepancy with the value predicted in the Standard Model, and relies on  $e^+e^-$  data for the computation of the hadronic loop contributions to the Standard Model value. The likelihood function is assumed to be Gaussian.

In each case, we run the `MultiNest` algorithm until we reach a sample of about  $3 \times 10^4$  points. Our focus in this work is to scan the parameter space of the new models, in order to study their phenomenology and identify regions compatible with the data. Performing any statistical (frequentist or Bayesian) interpretation of our results, based on global fits and confidence or credibility level regions, is beyond the scope of this paper and would require samples that are orders of magnitude larger than the ones we have gathered. Instead, we present scatter plots showing the correlations of pairs of parameters and/or observables in various planes. In doing this, we select from the full samples only those points predicting the value of all the observables within the  $2\sigma$  interval (with  $\sigma$  obtained by summing in quadrature the experimental and theoretical errors as explained in the previous paragraphs). If for the observable only an experimental exclusion limit exists, then the theoretical value is required to be within the 90/95 % CL exclusion limits. After applying these cuts, the number of points in the samples is substantially reduced. In particular, in none of the GUT models do we find points with a supersymmetric contribution to  $\delta a_\mu$  within the  $2\sigma$  interval. However, we highlight the points in our samples whose contributions to the anomalous magnetic moment of the muon lie in the  $3\sigma$  interval. We discuss this issue in Section 5.

## 4 Non-Universality Parameters and Relic Density Mechanisms

It is well known that, if the required amount of relic dark matter is provided by neutralinos, then particular mass relations must be present in the supersymmetric spectrum. In addition to mass relations, we use the neutralino composition to classify the relevant points of the supersymmetric parameter space. The higgsino fraction of the lightest neutralino mass eigenstate is characterized by the quantity

$$h_f \equiv |N_{13}|^2 + |N_{14}|^2, \quad (11)$$

where the  $N_{ij}$  are the elements of the unitary mixing matrix that correspond to the higgsino mass states. Thus, we classify the points that pass the constraints discussed in Section 2 according to the following criteria:

**Higgsino  $\chi_1^0$ :**

$$h_f > 0.1, \quad |m_A - 2m_\chi| > 0.1 m_\chi. \quad (12)$$

In this case, the lightest neutralino is higgsino-like and, as we discuss later, the lightest chargino  $\chi_1^\pm$  is almost degenerate in mass with  $\chi_1^0$ . The couplings to the SM gauge bosons are not suppressed and  $\chi_1^0$  pairs have large cross sections for annihilation into  $W^+W^-$  and  $ZZ$  pairs, which may reproduce the observed value of the relic abundance. Clearly, coannihilation channels involving  $\chi_1^\pm$  and  $\chi_2^0$  also contribute.

**$A/H$  resonances:**

$$|m_A - 2m_\chi| \leq 0.1 m_\chi. \quad (13)$$

The correct value of the relic abundance is achieved thanks to  $s$ -channel annihilation, enhanced by the resonant  $A$  propagator. The thermal average  $\langle \sigma_{ann} v \rangle$  spreads out the peak in the cross section, so that neutralino masses for which  $2m_\chi \simeq m_A$  is not exactly realized can also experience resonant annihilations.

**$\tilde{\tau}$  coannihilations:**

$$h_f < 0.1, \quad (m_{\tilde{\tau}_1} - m_\chi) \leq 0.1 m_\chi \quad (14)$$

The neutralino is bino-like, annihilation into leptons through  $t$ -channel slepton exchange is suppressed, and coannihilations involving the nearly-degenerate  $\tilde{\tau}_1$  are necessary to enhance the thermal-averaged effective cross section.

**$\tilde{\tau} - \tilde{\nu}_\tau$  coannihilations:**

$$h_f < 0.1, \quad (m_{\tilde{\tau}_1} - m_\chi) \leq 0.1 m_\chi, \quad (m_{\tilde{\nu}_\tau} - m_\chi) \leq 0.1 m_\chi. \quad (15)$$

Similar to the previous case, but also the  $\nu_{\tilde{\tau}}$  is nearly degenerate in mass with the  $\tilde{\tau}_1$ .

**$\tilde{t}_1$  coannihilations:**

$$h_f < 0.15, \quad (m_{\tilde{t}_1} - m_\chi) \leq 0.1 m_\chi. \quad (16)$$

The  $\tilde{t}_1$  is light and nearly degenerate with the bino-like neutralino. These coannihilations are present in the flipped SU(5) model.

We have performed the parameter-space scans in the three GUT groups with two different sets of ranges, as detailed in Table 1. The first one (Set 1) is broader, sampling soft terms up to 10 TeV and all the  $x_i$  in the ranges  $0 < x_i < 2$ . The MultiNest sampling of Set 1 finds that the data are more easily accommodated with a heavy spectrum, where the higgsino neutralino and  $A$  funnel mechanisms dominate and only few points in the coannihilation areas are found within the  $3 \times 10^4$  points sample.

Therefore, in order to zoom in the low mass spectrum, where coannihilations are expected to show up and is also favoured by the  $\delta a_\mu$  constraint, we performed a separate scan (Set 2), where we decrease the upper limits on  $m_0$  and  $m_{1/2}$ . Furthermore, the ranges of the parameters  $x_i$  are also restricted, since the coannihilation regions depend on the values of the  $x_i$  in a known way, as we explain below.

In the following plots, the points corresponding to the above mechanisms will be presented using different symbols and colours, as specified in the legend of Fig. 1. Although, in the scatter plots that we present, points of different types appear superimposed, we found that by applying the selection rules (12)-(16) to the whole samples, the obtained sets do not intersect. Only a few points that have  $h_f > 0.1$  and do not satisfy any of the above conditions are found in the Set 1 scans. These points lie in the areas of both the  $A/H$  resonances and a higgsino-like neutralino. Since they do not form a distinct region, they will not be shown in the figures, for reasons of clarity.

Fig. 1 shows the correlations between the non-universal parameters and the relic density mechanisms for each GUT group. The parameter  $x_d$  has no particular correlation with the above mechanisms, while in all cases higgsino DM corresponds to  $x_u > 1$ , and the same is also true for almost all the  $A/H$  funnel points, as seen in the upper left, upper right and lower left panels of Fig. 1. These mechanisms are independent from the GUT model choice, because the Higgs mass

Set 1	SO(10)	SU(5)	FSU(5)
$100 \text{ GeV} \leq m_0 \leq 10 \text{ TeV}$	$0 \leq x_u \leq 2$	$0 \leq x_u \leq 2$	$0 \leq x_u \leq 2$
$50 \text{ GeV} \leq m_{1/2} \leq 10 \text{ TeV}$	$0 \leq x_d \leq 2$	$0 \leq x_d \leq 2$	$0 \leq x_d \leq 2$
$-10 \text{ TeV} \leq A_0 \leq 10 \text{ TeV}$		$0 \leq x_5 \leq 2$	$0 \leq x_5 \leq 2$
$2 \leq \tan \beta \leq 65$			$0 \leq x_R \leq 2$
Set 2	SO(10)	SU(5)	FSU(5)
$100 \text{ GeV} \leq m_0 \leq 2500 \text{ GeV}$	$0 \leq x_u \leq 1$	$0 \leq x_u \leq 1$	$0 \leq x_u \leq 1$
$50 \text{ GeV} \leq m_{1/2} \leq 2500 \text{ GeV}$	$0 \leq x_d \leq 2$	$0 \leq x_d \leq 2$	$0 \leq x_d \leq 2$
$-10 \text{ TeV} \leq A_0 \leq 10 \text{ TeV}$		$0 \leq x_5 \leq 2$	$0 \leq x_5 \leq 1$
$2 \leq \tan \beta \leq 65$			$1 \leq x_R \leq 2$

Table 1: Sets of ranges used to sample the parameter spaces of the GUT models defined in Section 2. See the text for the definitions of the non-universality parameters  $x_i$ .

parameters follow the same pattern in the three scenarios. They are also influenced by the other soft terms due to renormalization group running, but this effect is not apparent in scatter plots like those presented here.

In SO(10) and SU(5) most of the  $\tilde{\tau}$  coannihilation points have  $x_u < 1$ . In SU(5), the flexibility allowed by the  $x_5$  parameter allows  $\tilde{\tau} - \tilde{\nu}$  coannihilations that are not present in SO(10). As seen in Fig. 1, these points lie in the  $x_5 < 1$  region. This is due to the fact that the lepton doublet belongs to the **5** representation while the quarks and the lepton singlet are in the **10**. Then, to satisfy the  $m_h$  constraint, the squark masses have to be large and the same is true for the right sleptons. However, left-slepton soft masses driven by a small value of  $x_5$  may lead to sleptons in the coannihilation range. The lower panels of Fig. 1 show that in the flipped SU(5)  $\tilde{\tau}$  and  $\tilde{\tau} - \tilde{\nu}$  coannihilations are located in the quadrants defined by  $x_u < 1$ ,  $x_5 < 1$ ,  $x_R > 1$ . We also see that a  $\tilde{t}$  coannihilation area is present. This is possible in flipped SU(5) because the right-handed squarks are in the  $\bar{\mathbf{5}}$  representation, so the stop mass decreases with  $x_5$ . On the other hand,  $x_R$  cannot be very small or the lightest stau becomes tachyonic. By restricting it to be  $> 1$  we avoid this situation, and also increase the left component in the lighter stau, since  $x_5 < x_R$ .

For simplicity and to avoid any discussion about cosmological constraints on tachyons, we consider here only positive values for  $m_{H_u}^2$  and  $m_{H_d}^2$  at the GUT scale. However, some negative values may be allowed, and have been included in some other analyses, leading to small differences. For example, in the case of the NUHM2 with  $m_{H_u}^2 \neq m_{H_d}^2 \neq m_0^2$ , the authors of [13] also consider negative values for  $m_0$ ,  $m_0^2$ ,  $m_{H_u}^2$ ,  $m_{H_d}^2$  and find their best fit point for  $m_0 < 0$ . In [57] the authors find a small stop island at 95% CL in the NUHM1 ( $m_{H_u}^2 = m_{H_d}^2 \neq m_0^2$ ) and a larger one in the NUHM2; this can be attributed to negative values of  $m_{H_u}^2$ , which enters in the RGE for  $m_{\tilde{t}_R}^2$  and decreases its value. Because of our restriction to positive values of  $x_u$  and  $x_d$ , in our analysis flipped SU(5) is the only scenario where this mass can become low for low values of  $x_5$ , due to its presence in the  $\bar{\mathbf{5}}$  instead of the **10**. In [28],  $M_A$  and  $\mu$  are taken as free parameters at low energies and the RGEs are used to obtain the corresponding GUT values for  $m_{H_u}^2$  and  $m_{H_d}^2$ , as described in [15]. This is a way to avoid sampling points that fail the electroweak symmetry breaking test. However, although some of these points correspond to negative values for  $m_{H_u}^2$  and/or  $m_{H_d}^2$ , the



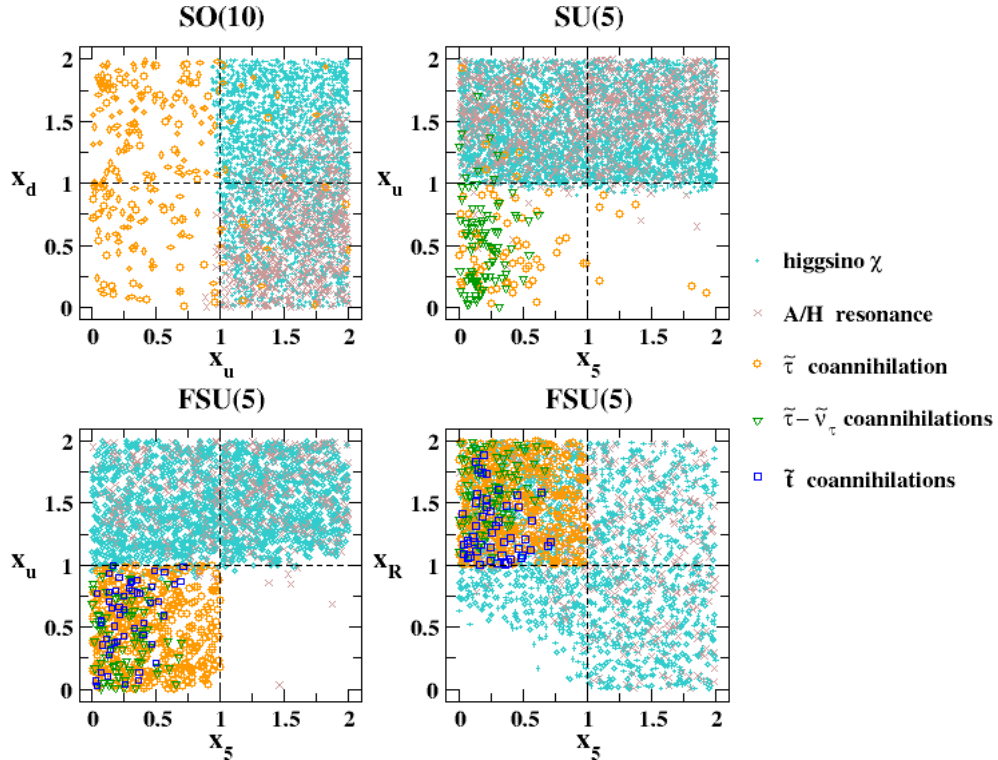


Figure 1: Correlations between the non-universal soft SUSY-breaking scalar mass parameters and the relic density mechanisms. The legend showing the meanings of colours and symbols for the points applies to all the figures of this paper.

authors do not display any region with stop coannihilations.

## 5 Relic Density, Higgs Mass and $\delta a_\mu^{SUSY}$

We now discuss in more detail the relations found in our scans between the relic abundance mechanisms, the value of the Higgs boson mass and the supersymmetric contribution to  $\delta a_\mu = [(g_\mu - 2)/2]_{\text{exp}} - [(g_\mu - 2)/2]_{\text{SM}}$ .

Most of the turquoise points in Fig. 2, with a higgsino  $\chi_1^0$  are confined in a thin strip with mass around 1 TeV, independently of the gauge group, and are only present in the upper panels of Fig. 1 where  $x_u > 1$ , as discussed previously. A higgsino-like neutralino with mass around 1 TeV is a general prediction driven by the relic density bound and has been emphasized before in many analysis [58], [59], [60], [61], [62].

Most of the  $A/H$  resonance points have a  $\chi_1^0$  mass larger than 800-900 GeV. They are numerous in the Set 1 scans (upper panels of Fig. 2), whereas they are reduced substantially in the Set 2 scans (lower panels of Fig. 2). In fact, for parameters within the ranges of Set 2, the  $A/H$  mass is smaller than in Set 1, therefore its decay width is smaller and the condition (13) is more difficult to respect.

The coannihilation areas are different in the various models and, as is well known, they feature upper limits on the  $\chi_1^0$  mass. In the case of SO(10), the  $\tilde{\tau}_1$  area (orange circles) is well defined, with the neutralino mass in the approximate interval 300-600 GeV. In the case of SU(5),  $\tilde{\tau}_1 - \tilde{\nu}_\tau$  coannihilations (green triangles) are also involved, and the upper limit increases to  $\sim 1.1$  TeV. The number of  $\tilde{\tau}_1$  points is reduced drastically in the Set 1 scan of flipped SU(5) and in the Set 2 scan

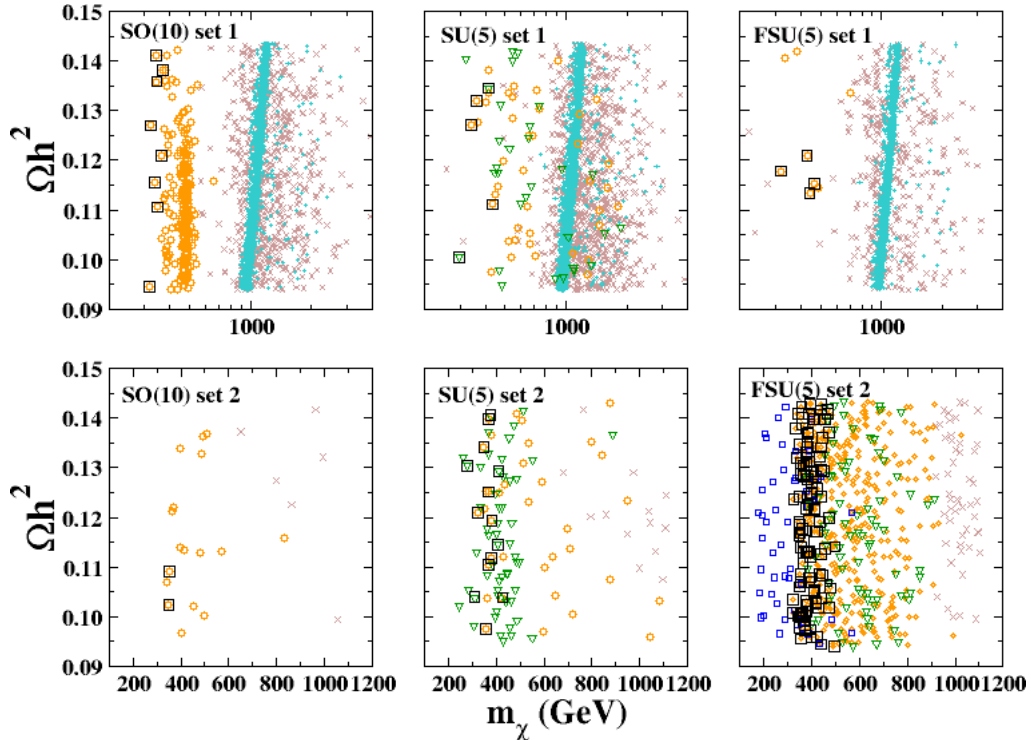


Figure 2: The neutralino relic density  $\Omega_\chi h^2$  as a function of the neutralino mass, using the symbols defined in the legend of Fig. 1. The points surrounded by black squares satisfy the constraint  $\delta a_\mu$  at  $3\sigma$ .

of SO(10). In the former case, the right-handed slepton mass is determined by the parameter  $x_R$ , which in Set 1 is free to vary over values larger than 1. In the latter case, the reduction is due to tension between the contribution to  $\delta a_\mu$ , which needs relatively light sleptons and gauginos, and a Higgs mass around 125 GeV, which pushes the preferred values of  $m_0$  and  $m_{1/2}$  towards higher values. The coannihilations in flipped SU(5) are recovered in the scan with Set 2, as seen in the bottom-right panel, where we also note the appearance of the  $\tilde{t}_1$  strip (dark blue squares). In SU(5) the situation is intermediate. The number of coannihilations does not vary so strongly, but in passing from Set 1 to Set 2 a greater concentration of points with light neutralino masses can be observed.

The black squares highlight the points for which the supersymmetric contribution to  $\delta a_\mu$  differs from the central value by less than  $3\sigma$ . The typical values of  $\delta a_\mu$  in the black squares are found to be in the range  $4 - 6 \times 10^{-10}$ , which is similar to the best-fit points in NUHM1 and NUHM2 models [12, 13]. All the black squares are in the region of  $\tilde{\tau}_1$  coannihilation, with a minority also featuring  $\tilde{\tau}_1 - \tilde{\nu}_\tau$  coannihilations. The scan with the largest number of  $\delta a_\mu$ -friendly points occurs in flipped SU(5) Set 2, due to the lightness of the spectrum and the additional freedom in the choice of parameters, as compared to SO(10) and SU(5).

In all our models, despite the larger freedom in the scalar sector allowed by the new parameters, it is hard to fully explain the  $\delta a_\mu$  anomaly with a supersymmetric contribution. In this respect the situation is thus similar to other models with gaugino and sfermion mass unification such as the CMSSM, NUHM1 and NUHM2 models [12, 13]. The difficulty to explain the anomaly at the  $2\sigma$  level in non-universal scalar GUT models was also recently discussed in [63], while, by relaxing also the condition of gaugino universality, the authors of [64] find models with supersymmetric contribution at  $2\sigma$ . Anyway, the GUT-boundary conditions employed in both these studies are

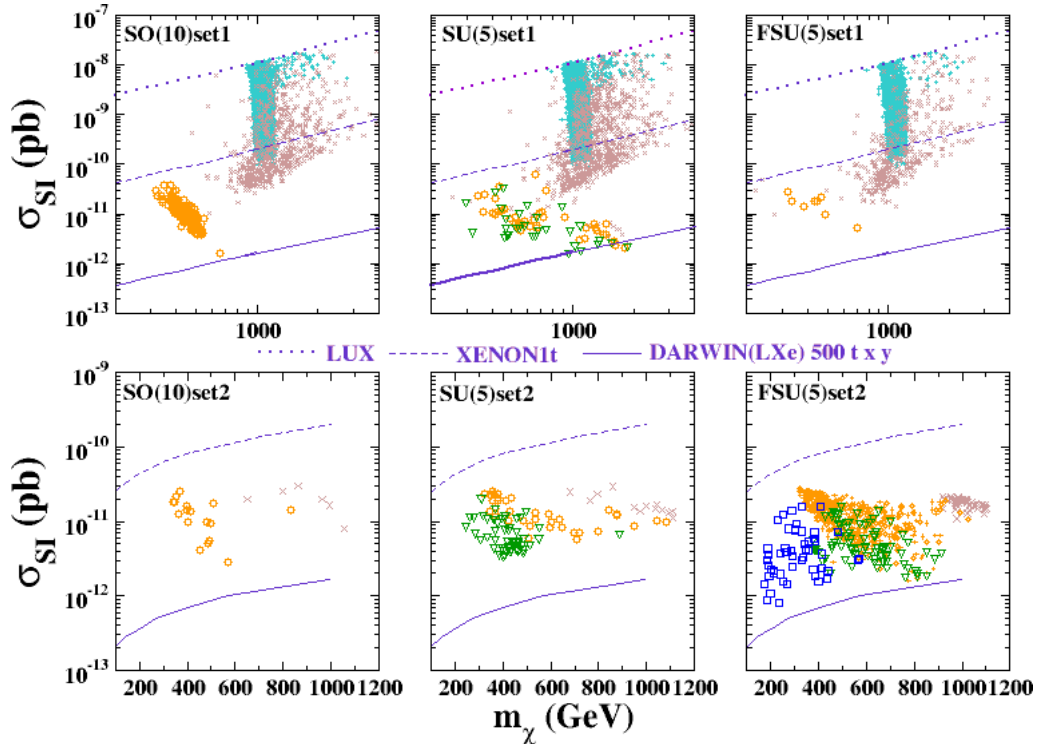


Figure 3: The spin-independent neutralino-nucleon cross section as a function of the neutralino mass. The dotted line is the current exclusion curve from the LUX experiment [49]. The projected sensitivities at 90% confidence level for the XENON 1 ton experiment [65, 66] (dashed line) and the DARWIN experiment [67] (full line) are taken from [68]. See the legend.

different from ours.

## 6 Direct and Indirect Dark Matter Searches

In Figure 3 we show scatter plots of the spin-independent neutralino-nucleon cross section as a function of the neutralino mass. The present limits from the null result of the LUX experiment [49] (dotted line) already exclude points with a higgsino-like neutralino and some points in the  $A/H$  funnel area. The projected sensitivity of the XENON 1 ton experiment [65, 66] shows that it could probe most of these areas, while coannihilations could be fully probed only with a multi-ton mass experiment like the DARWIN project [67], with an exposure of  $500 t \times y$ . These sensitivity curves are deduced from the recent study in [68].

We also show in Fig. 4 the present situation of the indirect dark matter search through  $\gamma$ -ray emission from annihilations in the halos of dwarf galaxies of the local group [69], by showing the total non-relativistic neutralino-neutralino annihilation cross section times the relative velocity in dark matter halos  $\sigma_{\text{ann}} v_r$  as a function of the neutralino mass. The three curves are all limits from the combined analysis of the FERMI satellite with 6 years of data [70] obtained assuming that  $\tau\bar{\tau}$ ,  $b\bar{b}$  and  $W\bar{W}$  final states dominate. Gamma rays may result from the decays and hadronization of any of these final states, and in principle these limits apply only to points where these channels dominate neutralino annihilation, and can therefore be compared with the higgsino and resonance regions. We see that at present the curves do not touch the favoured regions of parameter space. Future data from FERMI or CTA arrays [61], [71] may possibly probe the turquoise and red points

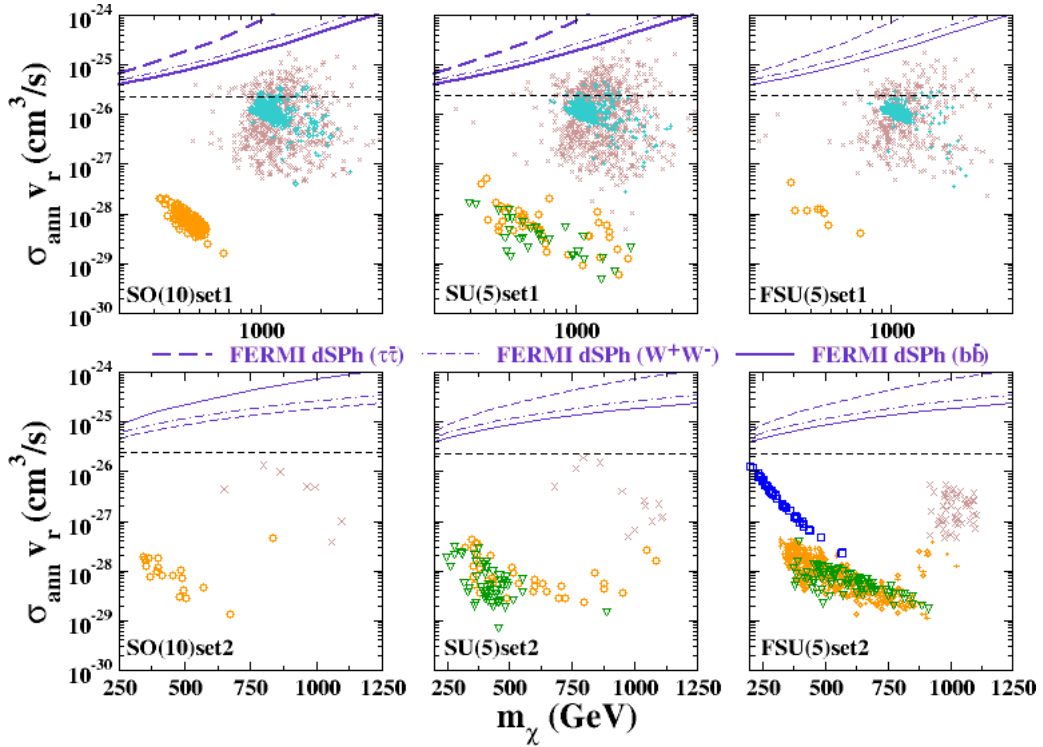


Figure 4: The total non-relativistic  $\chi_1^0$  annihilation cross section times relative velocity as a function of the neutralino mass. The purple lines are the present exclusion limits from a FERMI analysis of gamma-ray emission from dwarf spheroidal galaxies [70]: see the legend for the specific final states. The horizontal black dashed line corresponds to the usual benchmark value of  $\langle\sigma_{\text{eff}}v_{\text{rel}}\rangle \simeq 2 - 3 \times 10^{-26} \text{ cm}^3/\text{s}$ .

(higgsino and  $A/H$  funnel regions). As could be expected, the annihilation cross section in the slepton coannihilation region is too small to be probed by this kind of indirect searches.

The dashed line corresponds to the usual benchmark value of  $\langle\sigma_{\text{eff}}v_{\text{rel}}\rangle \simeq 2 - 3 \times 10^{-26} \text{ cm}^3/\text{s}$  for a weakly-interacting massive particle with a relic abundance  $\Omega h^2 \simeq 0.1$ . We remark that the values of  $\sigma_{\text{ann}}v_r$  shown in Figure 4 coincide with those of the thermal average at freeze-out  $\langle\sigma_{\text{eff}}v_{\text{rel}}\rangle$  only when there are no coannihilation channels and the product  $\sigma_{\text{ann}}v_r$  is a constant independent from the relative velocity/temperature at freeze-out.

## 7 LHC Searches

**LHC missing energy searches:** The coannihilation areas yield a light supersymmetric spectrum that is already partially probed by the first years of operation of LHC. In Figs. 5 and 6, we show the distributions in the  $(m_{1/2}, m_0)$  and  $(m_{\tilde{q}}, m_{\tilde{g}})$  planes for the various GUT models. The present LHC 95 % CL exclusion limit from missing  $E_T$  searches [57] are depicted as solid lines, while the projected sensitivity with  $300 \text{ fb}^{-1}$  at 14 TeV [57] is represented by dashed lines. We see that the present exclusion limits already constrain the  $t$ -coannihilation area of flipped SU(5) (blue squares), and graze the  $\tilde{\tau}$ -coannihilation points favoured by the  $\delta a_\mu$  constraint in all GUT models. The projected LHC missing  $E_T$  sensitivity covers most of the coannihilation areas, but leaves practically untouched the higgsino and resonance areas.

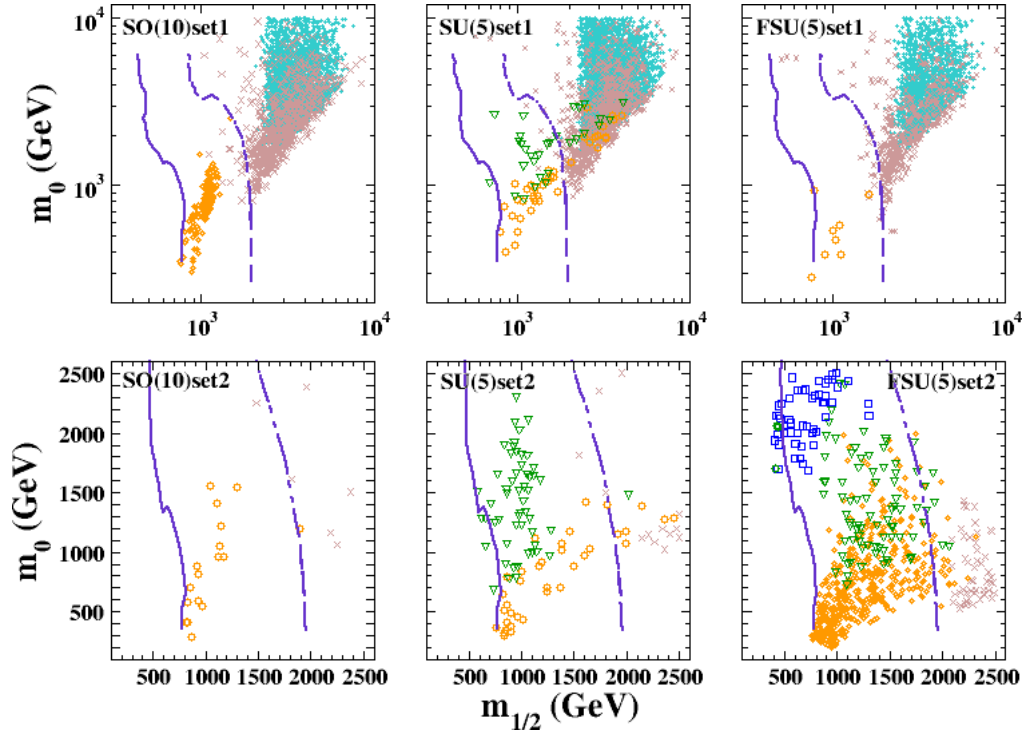


Figure 5: Scatter plots of non-universal GUT models in the  $(m_{1/2}, m_0)$  plane, with the same legend as in Fig. 1. The current LHC 95 % CL exclusion (solid purple line) and the projected exclusion sensitivity at 14 TeV with  $300 \text{ fb}^{-1}$  (dashed purple line) are taken from Ref. [57].

**Heavy Higgs and charginos:** We now discuss the sensitivity of other search channels at the LHC to supersymmetric particles in the models we study. The present exclusion curve in the  $(\tan \beta, m_A)$  plane is shown as a solid purple line in Fig. 7. We see that the mass of the pseudoscalar neutral Higgs  $A$  is generally larger than 1 TeV, except for a few points in the higgsino and resonance regions, which are excluded by this constraint. If the sensitivity in this plane could be pushed to masses up to 2-2.5 TeV, most of the  $\tilde{\tau}_1$  coannihilation areas could be probed, as seen in the lower panels of Fig. 7.

More interesting is the search for the lighter chargino,  $\chi_1^\pm$ , shown in the  $(m_\chi, m_{\chi_1^\pm})$  plane in Fig. 8. In the Set 1 scans (upper plots), the points are distributed in the region where  $m_\chi \lesssim m_{\chi_1^\pm} \lesssim 2m_\chi$ . In the coannihilation regions, the neutralino is bino-like,  $m_\chi \simeq M_1$ , whereas the chargino is gaugino-like with  $m_{\chi_1^\pm} \simeq M_2 \simeq 2M_1 \simeq 2M_1$ . On the other hand, for a higgsino-like neutralino, we have  $m_\chi \simeq \mu$ , since the mass of the lightest chargino is dominated by the  $\mu$  mass parameter. The  $A/H$  funnel resonance, with bino-higgsino neutralino mixing, lies in the area between the two extreme cases above. This behaviour results from the interplay between the universality of the gaugino masses at the GUT scale and constraints imposed by the relic abundance.

The solid indigo line is the present limit from the search for  $\chi_1^\pm \chi_2^0$  production and decays into  $W/Z$  and missing  $E_T$ , and the solid red line shows the limit from the search for gaugino pair production  $\chi_1^\pm \chi_2^0, \chi_1^\pm \chi_1^\pm$ , with multi- $\tau$  final-state decays and missing energy. In both cases, the dashed lines indicate the projected sensitivity with  $3000 \text{ fb}^{-1}$  at 14 TeV: all the limits are taken from Refs. [72], [57]. In the latter channel, the LHC will be able to probe parts of the  $\tilde{\tau}_1$  coannihilation strips (orange circles and green triangles) and, in the case of the flipped SU(5), most of the  $\tilde{t}_1$  coannihilation strip.

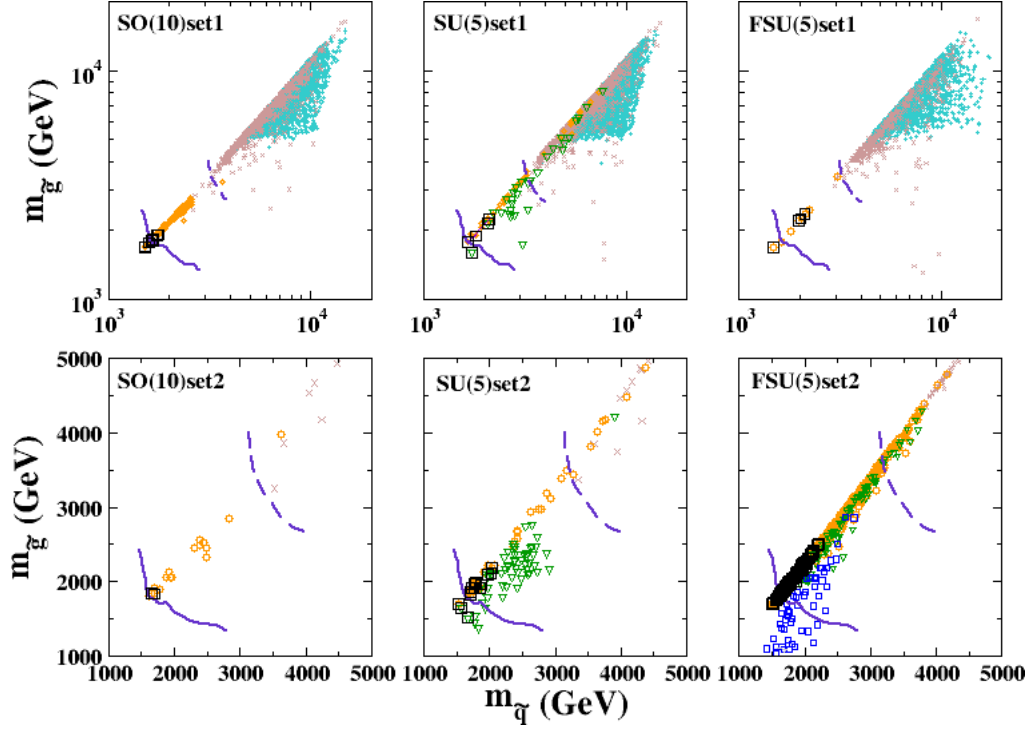


Figure 6: Scatter plots of non-universal GUT models in the  $(m_{\tilde{q}}, m_{\tilde{g}})$  plane, with the same legend as in Fig. 1. The current LHC 95 % CL exclusion (solid purple line) and the projected exclusion sensitivity at 14 TeV with  $300 \text{ fb}^{-1}$  (dashed purple line) are taken from Ref. [57].

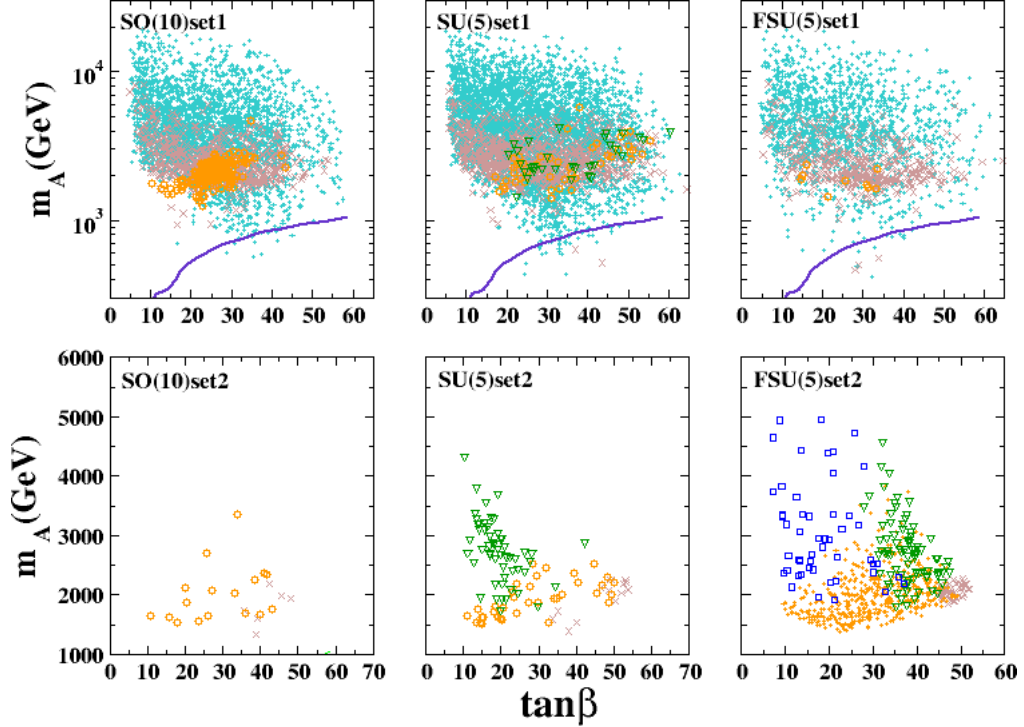


Figure 7: Scatter plots of non-universal GUT models in the  $(\tan \beta, m_A)$  plane, with the same legend as in Fig. 1. The current LHC 95 % CL exclusion (solid purple line) is taken from [57].

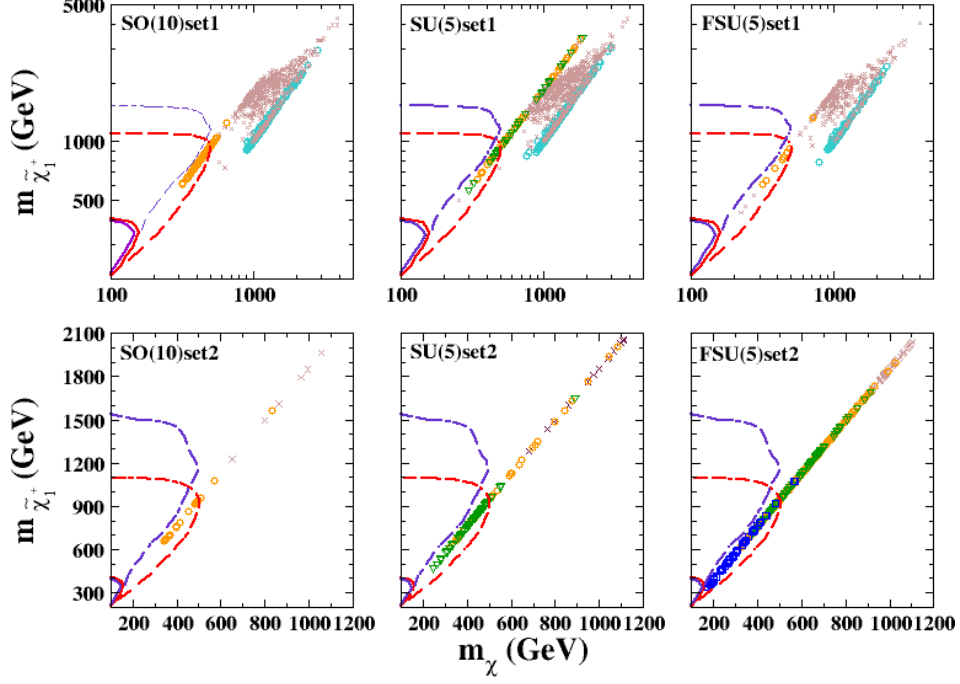


Figure 8: Scatter plots of non-universal GUT models in the  $(m_\chi, m_{\tilde{\chi}_1^\pm})$  plane, with the same legend as in Fig. 1. The current LHC 95 % CL exclusion (solid purple line) and projected sensitivity (dashed purple line) are taken from [57]. See the text for details. The projected lines correspond to the sensitivity with  $3000 \text{ fb}^{-1}$ .

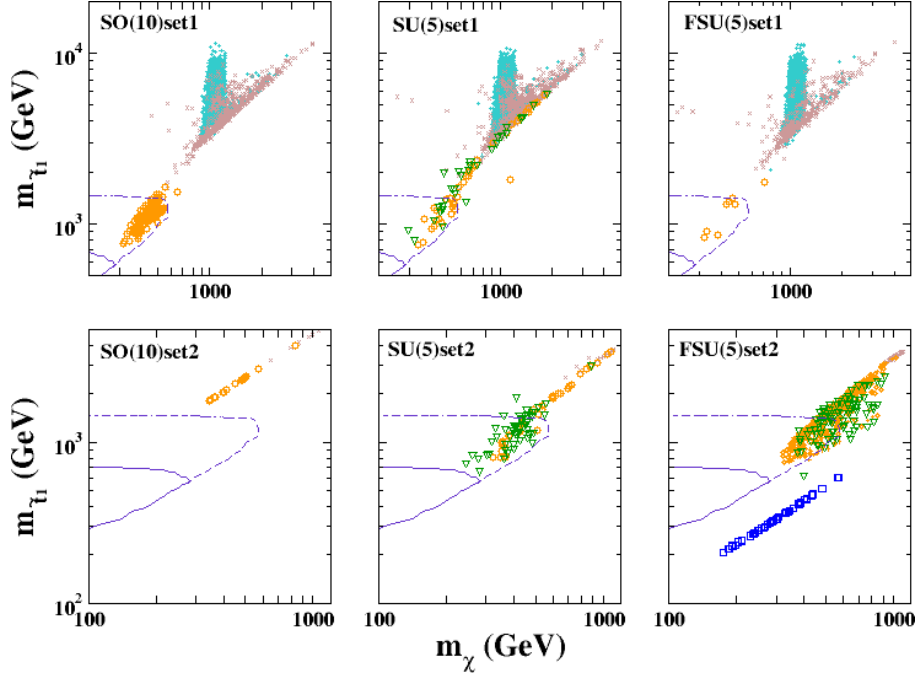


Figure 9: Scatter plots of non-universal GUT models in the  $(m_\chi, m_{\tilde{\tau}_1})$  plane, with the same legend as in Fig. 1. The solid and dashed purple lines are the present limit and projected sensitivity [73, 74, 57]. See the text for details. The projected line corresponds to the sensitivity with  $3000 \text{ fb}^{-1}$ .

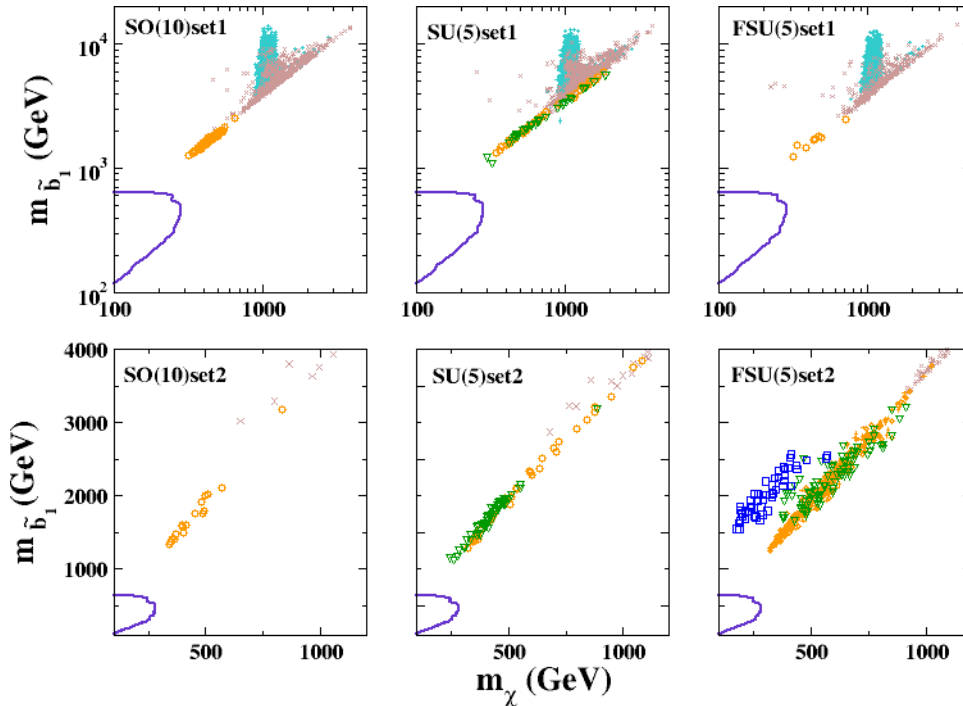


Figure 10: Scatter plots of non-universal GUT models in the  $(m_{\chi}, m_{\tilde{b}_1})$  plane, with the same legend as in Fig. 1. The solid purple line is the ATLAS 95 %CL limit from [73, 74]. See the text for details.

**Third-Generation Squarks:** As seen in Fig. 9, the stop mass in the models we study is generally larger than 800 GeV, and the present limits from searches in  $\tilde{t}_1 \rightarrow t\chi_1^0$ , do not reach such values. On the other hand, the projected sensitivity with  $3000 \text{ fb}^{-1}$  will partly cover the  $\tilde{\tau}_1$  coannihilation regions. The flipped SU(5) Set 2 scan displays the stop coannihilation strip where both the  $\tilde{t}_1$  and neutralino mass are in the range 200-600 GeV. However, we see that the  $\tilde{t}_1$  strip is not affected by the above-mentioned search, though we have already seen that it is constrained indirectly by the limits in Figs. 5, 6 and 8.

We see in Fig. 10 that the lighter sbottom squark is heavier than 1 TeV in all the panels. The present 95 %CL limit for  $\tilde{b}_1$  pair production decaying to  $b\chi$  [73, 74] does not reach the favoured regions, and the searches for this sparticle are not competitive with the other channels.

**Complementarity of searches:** Under the assumption that the lightest neutralino constitutes all the observed relic abundance, Figs. 3, 4, 5 and 6 show the complementarity of dark matter experiments and of LHC searches for supersymmetric particles. The GUT-inspired models and their respective parameter spaces, as studied in our work, can be fully probed or excluded by combining  $300 \text{ fb}^{-1}$  of data accumulated by missing energy LHC searches (coannihilation areas), with the next generation of ton-scale direct-detection experiments. This is consistent with the results of [61], [57], where similar complementarity was found in studies of the CMSSM, NUHM1, NUHM2 and pMSSM10.

## 8 Summary and Conclusions

In the following, we summarize the principal conclusions of this work.



- We have identified different patterns of soft SUSY-breaking terms at the GUT scale, depending on the grand unification group, which we have used to distinguish different GUT scenarios via their dark matter predictions and the constraints from LHC searches.
- We have calculated the SUSY spectra for the different gauge groups, finding that the models predict different spectra for the same LSP mass, connecting possible future observations with the structure of the underlying unified theory.
- None of the GUT models studied offers high prospects for reducing substantially the  $a_\mu$  discrepancy via a SUSY contribution.
- In general, scenarios that favour degeneracies in the sparticle spectrum lead to additional contributions to coannihilations, thus enhancing the efficiency and importance of these processes.
- We have studied the different relic density predictions and determined upper bounds for the neutralino mass in the different GUT scenarios. We have also computed the cross sections for direct and indirect dark matter detection in each case, combining the bounds from different dark matter experiments with those from LHC searches.
- We have found that SO(10), SU(5) and flipped SU(5) lead to very different predictions for dark matter and LHC experiments, and thus are distinguishable in future searches. Among other differences, flipped SU(5) predicts  $\tilde{t}_1 - \chi$  coannihilations that are absent in the other groups within the parameter ranges studied here, but can be explored by LHC searches.
- Direct searches for astrophysical dark matter scattering show interesting prospects for the Xenon 1 ton and Darwin experiments, and models with a higgsino-like LSP or  $A/H$  resonance annihilation may offer prospects for future FERMI or CTA  $\gamma$ -ray searches.
- The LHC searches for generic missing  $E_T$ , charginos and stops are quite complementary, and future LHC runs will be able to constrain the models in several different ways.

The interesting prospects for exploring the parameter spaces of different SUSY GUT models found in this paper, and the fact that their potential signatures are quite distinctive, whet our appetites for data from LHC Run 2 and searches for astrophysical dark matter.

## Acknowledgements

The work of J.E. has been supported in part by the European Research Council via the Advanced Investigator Grant 267352, and by the UK STFC via the research grant ST/L000326/1. The work of M.C. has been supported in part by the MINECO grant FPA2011-23778 and by the MINECO/FEDER research grant CPI-14-397, and acknowledges A. Pich, G. Rodrigo, J. Portolés, P. Hernández and N. Rius for hospitality at IFIC in Valencia where part of this work was done. M.C. and M.E.G. acknowledge support from the MINECO grant: "Fenomenología en Física de Partículas y Astropartículas" (FPA2014-53631). S.L. thanks CERN for kind hospitality. R. RdA is supported by the Ramón y Cajal program of the Spanish MICINN, by the Invisibles European ITN project (FP7-PEOPLE-2011-ITN, PITN-GA-2011-289442-INVISIBLES), and by the MEC projects "SOM: Sabor y origen de la Materia" (2014-57816) and "Fenomenología y Cosmología de la Física mas allá del Modelo Estándar e implicaciones Experimentales en la era del LHC" (FPA2013-44773). M.C., M.E.G. and R.RdA acknowledge support from Spanish MICINN Consolider-Ingenio 2010 Program under the grant MULTIDARK CSD2209-00064.

## References

- [1] G. Aad *et al.* [ATLAS Collaboration], “*Observation of a new particle in the search for the Standard Model Higgs boson with the ATLAS detector at the LHC,*” Phys. Lett. B **716** 1 (2012) [1207.7214].
- [2] S. Chatrchyan *et al.* [CMS Collaboration], “*Observation of a new boson at a mass of 125 GeV with the CMS experiment at the LHC,*” Phys. Lett. B **716** 30 (2012) [1207.7235].
- [3] G. Aad *et al.* [ATLAS and CMS Collaborations], “*Combined Measurement of the Higgs Boson Mass in  $pp$  Collisions at  $\sqrt{s} = 7$  and 8 TeV with the ATLAS and CMS Experiments,*” Phys. Rev. Lett. **114** 191803 (2015) [1503.07589].
- [4] ATLAS and CMS Collaborations, “*Measurements of the Higgs boson production and decay rates and constraints on its couplings from a combined ATLAS and CMS analysis of the LHC  $pp$  collision data at  $\sqrt{s} = 7$  and 8 TeV,*” ATLAS-CONF-2015-044, CMS-PAS-HIG-15-002, <https://cds.cern.ch/record/2052552/files/ATLAS-CONF-2015-044.pdf>.
- [5] H. Goldberg, “*Constraint on the Photino Mass from Cosmology,*” Phys. Rev. Lett. **50**, 1419 (1983);
- [6] J. Ellis, J. Hagelin, D. Nanopoulos, K. Olive and M. Srednicki, “*Supersymmetric Relics from the Big Bang,*” Nucl. Phys. B **238**, 453 (1984).
- [7] E. Komatsu *et al.* [WMAP Collaboration], “*Seven-Year Wilkinson Microwave Anisotropy Probe (WMAP) Observations: Cosmological Interpretation,*” Astrophys. J. Suppl. **192**, 18 (2011) [1001.4538].
- [8] C. L. Bennett *et al.* [WMAP Collaboration], “*Nine-Year Wilkinson Microwave Anisotropy Probe (WMAP) Observations: Final Maps and Results,*” Astrophys. J. Suppl. **208**, 20 (2013) [1212.5225].
- [9] P. A. R. Ade *et al.* [Planck Collaboration], “*Planck 2013 results. XVI. Cosmological parameters,*” Astron. Astrophys. **571**, A16 (2014) [1303.5076].
- [10] P. A. R. Ade *et al.* [Planck Collaboration], “*Planck 2015 results. XIII. Cosmological parameters,*” arXiv:1502.01589.
- [11] J. Ellis and K. A. Olive, “*Revisiting the Higgs Mass and Dark Matter in the CMSSM,*” Eur. Phys. J. C **72**, 2005 (2012) [1202.3262].
- [12] O. Buchmueller *et al.*, “*The CMSSM and NUHM1 after LHC Run 1,*” Eur. Phys. J. C **74**, 2922 (2014) [1312.5250].
- [13] O. Buchmueller *et al.*, “*The NUHM2 after LHC Run 1,*” Eur. Phys. J. C **74**, 3212 (2014) [1408.4060].
- [14] C. Strege, G. Bertone, F. Feroz, M. Fornasa, R. Ruiz de Austri and R. Trotta, “*Global Fits of the  $m$ SSM and NUHM including the LHC Higgs discovery and new XENON100 constraints,*” JCAP **1304** 013 (2013) [1212.2636].
- [15] H. Baer, A. Mustafayev, S. Profumo, A. Belyaev and X. Tata, “*Direct, indirect and collider detection of neutralino dark matter in SUSY models with non-universal Higgs masses,*” JHEP **0507** (2005) 065 [hep-ph/0504001].
- [16] L. Roszkowski, R. Ruiz de Austri, R. Trotta, Y. L. S. Tsai and T. A. Varley, “*Global fits of the Non-Universal Higgs Model,*” Phys. Rev. D **83**, 015014 (2011) [Phys. Rev. D **83**, 039901 (2011)] [0903.1279].
- [17] B. Ananthanarayan, G. Lazarides and Q. Shafi, “*Top mass prediction from supersymmetric guts,*” Phys. Rev. D **44** (1991) 1613.

- [18] S. Dimopoulos, L. J. Hall and S. Raby, “*A Predictive framework for fermion masses in supersymmetric theories,*” Phys. Rev. Lett. **68** (1992) 1984.
- [19] S. Dimopoulos, L. J. Hall and S. Raby, “*A Predictive ansatz for fermion mass matrices in supersymmetric grand unified theories,*” Phys. Rev. D **45** (1992) 4192.
- [20] M. Carena, S. Dimopoulos, C. E. M. Wagner and S. Raby, “*Fermion masses, mixing angles and supersymmetric  $SO(10)$  unification,*” Phys. Rev. D **52**, 4133 (1995) [hep-ph/9503488].
- [21] M. Carena, J. R. Ellis, S. Lola and C. E. M. Wagner, “*Neutrino masses, mixing angles and the unification of couplings in the MSSM,*” Eur. Phys. J. C **12**, 507 (2000) [hep-ph/9906362].
- [22] H. Georgi and S. L. Glashow, “*Unity of All Elementary Particle Forces,*” Phys. Rev. Lett. **32**, 438 (1974);
- [23] S. Dimopoulos and H. Georgi, “*Softly Broken Supersymmetry and  $SU(5)$ ,*” Nucl. Phys. B **193**, 150 (1981).
- [24] S. M. Barr, “*A New Symmetry Breaking Pattern for  $SO(10)$  and Proton Decay,*” Phys. Lett. B **112**, 219 (1982).
- [25] J. P. Derendinger, J. E. Kim and D. V. Nanopoulos, “*Anti- $SU(5)$ ,*” Phys. Lett. B **139**, 170 (1984).
- [26] I. Antoniadis, J. R. Ellis, J. S. Hagelin and D. V. Nanopoulos, “*Supersymmetric Flipped  $SU(5)$  Revitalized,*” Phys. Lett. B **194**, 231 (1987).
- [27] J. Ellis, A. Mustafayev and K. A. Olive, “*Constrained Supersymmetric Flipped  $SU(5)$  GUT Phenomenology,*” Eur. Phys. J. C **71**, 1689 (2011) [1103.5140].
- [28] N. Okada, S. Raza and Q. Shafi, “*Particle Spectroscopy of Supersymmetric  $SU(5)$  in Light of 125 GeV Higgs and Muon  $g-2$  Data,*” Phys. Rev. D **90**, 015020 (2014) [1307.0461].
- [29] C. Pallis, “ *$b$   $\tau$  unification with gaugino and sfermion mass nonuniversality,*” Nucl. Phys. B **678**, 398 (2004) [hep-ph/0304047].
- [30] F. Feroz, M. P. Hobson and M. Bridges, “*MultiNest: an efficient and robust Bayesian inference tool for cosmology and particle physics,*” Mon. Not. Roy. Astron. Soc. **398**, 1601 (2009) [0809.3437].
- [31] <http://www.ft.uam.es/personal/rruiz/superbayes>
- [32] <http://projects.hepforge.org/softsusy/>
- [33] B. C. Allanach, “*SOFTSUSY: a program for calculating supersymmetric spectra,*” Comput. Phys. Commun. **143** (2002) 305 [hep-ph/0104145].
- [34] <http://lapth.in2p3.fr/micromegas/>
- [35] G. Belanger, F. Boudjema, A. Pukhov and A. Semenov, “*micrOMEGAs2.0: A program to calculate the relic density of dark matter in a generic model,*” Comput. Phys. Commun. **176** (2007) 367 [hep-ph/0607059].
- [36] P. Gondolo, J. Edsjö, P. Ullio, L. Bergström, M. Schelke, E.A. Baltz, T. Bringmann and G. Duda, <http://www.darksusy.org/>
- [37] P. Gondolo, J. Edsjo, P. Ullio, L. Bergstrom, M. Schelke and E. A. Baltz, “*DarkSUSY: Computing supersymmetric dark matter properties numerically,*” JCAP **0407** (2004) 008 [astro-ph/0406204].
- [38] <http://superiso.in2p3.fr/>
- [39] F. Mahmoudi, “*SuperIso v2.3: A Program for calculating flavor physics observables in Supersymmetry,*” Comput. Phys. Commun. **180**, 1579 (2009) [0808.3144].

- [40] <http://slavich.web.cern.ch/slavich/susybsg/>
- [41] G. Degrandi, P. Gambino and P. Slavich, “*SusyBSG: a fortran code for BR[B -j Xs gamma] in the MSSM with Minimal Flavor Violation,*” *Comput. Phys. Commun.* **179** (2008) 759 [0712.3265].
- [42] S. Schael *et al.* [ALEPH and DELPHI and L3 and OPAL and SLD and LEP Electroweak Working Group and SLD Electroweak Group and SLD Heavy Flavour Group Collaborations], “*Precision electroweak measurements on the Z resonance,*” *Phys. Rept.* **427**, 257 (2006) [hep-ex/0509008].
- [43] K. A. Olive *et al.* [Particle Data Group Collaboration], “*Review of Particle Physics,*” *Chin. Phys. C* **38**, 090001 (2014).
- [44] C. Strege, G. Bertone, G. J. Besjes, S. Caron, R. Ruiz de Austri, A. Strubig and R. Trotta, “*Profile likelihood maps of a 15-dimensional MSSM,*” *JHEP* **1409**, 081 (2014) [1405.0622].
- [45] A. Arbey, M. Battaglia, F. Mahmoudi and D. Martínez Santos, “*Supersymmetry confronts  $B_s^{+-}$  : Present and future status,*” *Phys. Rev. D* **87**, no. 3, 035026 (2013) [1212.4887].
- [46] V. Khachatryan *et al.* [CMS and LHCb Collaborations], “*Combination of results on the rare decays  $B_{(s)}^0 \rightarrow \mu^+ \mu^-$  from the CMS and LHCb experiments,*” CMS-PAS-BPH-13-007, LHCb-CONF-2013-012, CERN-LHCb-CONF-2013-012;
- [47] V. Khachatryan *et al.* [CMS and LHCb Collaborations], “*Observation of the rare  $B_s^0 \rightarrow \mu^+ \mu^-$  decay from the combined analysis of CMS and LHCb data,*” *Nature* **522**, 68 (2015) [1411.4413].
- [48] P. A. R. Ade *et al.* [Planck Collaboration], “*Planck 2013 results. XVI. Cosmological parameters,*” *Astron. Astrophys.* **571**, A16 (2014) [1303.5076].
- [49] D. S. Akerib *et al.* [LUX Collaboration], “*First results from the LUX dark matter experiment at the Sanford Underground Research Facility,*” *Phys. Rev. Lett.* **112**, 091303 (2014) [1310.8214].
- [50] C. Savage, A. Scaffidi, M. White and A. G. Williams, “*LUX likelihood and limits on spin-independent and spin-dependent WIMP couplings with LUXCalc,*” arXiv:1502.02667.
- [51] G. S. Bali *et al.* [QCDSF Collaboration], “*Strangeness Contribution to the Proton Spin from Lattice QCD,*” *Phys. Rev. Lett.* **108**, 222001 (2012) [1112.3354].
- [52] P. Junnarkar and A. Walker-Loud, “*Scalar strange content of the nucleon from lattice QCD,*” *Phys. Rev. D* **87**, 114510 (2013) [1301.1114].
- [53] P. Bechtle, O. Brein, S. Heinemeyer, O. Stål, T. Stefaniak, G. Weiglein and K. E. Williams, “*HiggsBounds – 4: Improved Tests of Extended Higgs Sectors against Exclusion Bounds from LEP, the Tevatron and the LHC,*” *Eur. Phys. J. C* **74**, no. 3, 2693 (2014) [1311.0055].
- [54] P. Bechtle, S. Heinemeyer, O. Stål, T. Stefaniak and G. Weiglein, “*HiggsSignals: Confronting arbitrary Higgs sectors with measurements at the Tevatron and the LHC,*” *Eur. Phys. J. C* **74**, 2711 (2014) [1305.1933].
- [55] R. R. de Austri, R. Trotta and L. Roszkowski, “*A Markov chain Monte Carlo analysis of the CMSSM,*” *JHEP* **0605**, 002 (2006) [hep-ph/0602028].
- [56] M. Davier, A. Hoecker, B. Malaescu and Z. Zhang, “*Reevaluation of the Hadronic Contributions to the Muon  $g-2$  and to  $\alpha(MZ)$ ,*” *Eur. Phys. J. C* **71**, 1515 (2011) [*Eur. Phys. J. C* **72**, 1874 (2012)] [1010.4180].
- [57] E. A. Bagnaschi *et al.*, “*Supersymmetric Dark Matter after LHC Run 1,*” *Eur. Phys. J. C* **75**, 500 (2015) [1508.01173].
- [58] K. A. Olive and M. Srednicki, “*Cosmological limits on massive LSP ’s,*” *Nucl. Phys. B* **355**, 208 (1991).

- [59] S. Profumo and C. E. Yaguna, “*A Statistical analysis of supersymmetric dark matter in the MSSM after WMAP,*” Phys. Rev. D **70**, 095004 (2004) [hep-ph/0407036].
- [60] U. Chattopadhyay, D. Choudhury, M. Drees, P. Konar and D. P. Roy, “*Looking for a heavy Higgsino LSP in collider and dark matter experiments,*” Phys. Lett. B **632**, 114 (2006) [hep-ph/0508098].
- [61] L. Roszkowski, E. M. Sessolo and A. J. Williams, “*What next for the CMSSM and the NUHM: Improved prospects for superpartner and dark matter detection,*” JHEP **1408**, 067 (2014) [1405.4289].
- [62] K. A. Olive, “*Supersymmetric Dark Matter after Run I at the LHC: From a TeV to a PeV,*” arXiv:1510.06412.
- [63] J. Chakraborty, A. Choudhury and S. Mondal, “*Non-universal Gaugino mass models under the lamppost of muon ( $g-2$ ),*” JHEP **1507**, 038 (2015) [1503.08703].
- [64] K. Kowalska, L. Roszkowski, E. M. Sessolo and A. J. Williams, “*GUT-inspired SUSY and the muon  $g-2$  anomaly: prospects for LHC 14 TeV,*” JHEP **1506**, 020 (2015) [1503.08219].
- [65] E. Aprile [XENON 1 ton Collaboration], “*The XENON1T Dark Matter Search Experiment,*” Springer Proc. Phys. **148**, 93 (2013) [1206.6288].
- [66] E. Aprile *et al.* [XENON Collaboration], “*Physics reach of the XENON1T dark matter experiment,*” [arXiv:1512.07501].
- [67] L. Baudis [DARWIN Consortium Collaboration], “*DARWIN: dark matter WIMP search with noble liquids,*” J. Phys. Conf. Ser. **375**, 012028 (2012) [1201.2402].
- [68] M. Schumann, L. Baudis, L. Bütikofer, A. Kish and M. Selvi, “*Dark matter sensitivity of multi-ton liquid xenon detectors,*” JCAP **1510**, 016 (2015) [1506.08309].
- [69] M. A. Sánchez-Conde, M. Cannoni, F. Zandanel, M. E. Gómez and F. Prada, “*Dark matter searches with Cherenkov telescopes: nearby dwarf galaxies or local galaxy clusters?,*” JCAP **1112**, 011 (2011) [1104.3530].
- [70] M. Ackermann *et al.* [Fermi-LAT Collaboration], “*Searching for Dark Matter Annihilation from Milky Way Dwarf Spheroidal Galaxies with Six Years of Fermi-LAT Data,*” arXiv:1503.02641.
- [71] J. Carr *et al.* [CTA Consortium Collaboration], “*Prospects for Indirect Dark Matter Searches with the Cherenkov Telescope Array (CTA),*” arXiv:1508.06128.
- [72] G. Aad *et al.* [ATLAS Collaboration], “*Search for the direct production of charginos, neutralinos and staus in final states with at least two hadronically decaying taus and missing transverse momentum in  $pp$  collisions at  $\sqrt{s} = 8$  TeV with the ATLAS detector,*” JHEP **1410**, 96 (2014) [1407.0350].
- [73] G. Aad *et al.* [ATLAS Collaboration], “*ATLAS Run 1 searches for direct pair production of third-generation squarks at the Large Hadron Collider,*” Eur. Phys. J. C **75**, 510 (2015) [1506.08616].
- [74] G. Aad *et al.* [ATLAS Collaboration], “*Search for direct third-generation squark pair production in final states with missing transverse momentum and two  $b$ -jets in  $\sqrt{s} = 8$  TeV  $pp$  collisions with the ATLAS detector,*” JHEP **1310**, 189 (2013) [1308.2631].